Multiscale modeling of unsaturated granular materials based on thermodynamic principles

Chao-Fa Zhao[1,2], Younes Salami[1,3], Pierre-Yves Hicher[1,*], Zhen-Yu Yin[1,4]

[1] *Institut de Recherche en Génie Civil et Mécanique (GeM), UMR CNRS 6183, Ecole Centrale de Nantes, 1 rue de la Noë, BP 92101, 44321 Nantes cedex 3, France.*

[2] *LaSIE-UMR CNRS 7356, Université de La Rochelle, 23 Avenue Albert Einstein, La Rochelle 17000, France.*

[3] *Euro-Mediterranean University of Fès (UEMF), route de Meknès, 30000 Fès, Morocco.*

[4] *Department of Civil and Environmental Engineering, The Hong Kong Polytechnic University, Hung Hom, Kowloon, Hong Kong.*

Abstract

The effect of water on the hydro-mechanical behavior of unsaturated granular materials has been studied with a micromechanical model based on thermodynamic principles. A general framework based on the theory of thermodynamics with internal variables for constructing thermodynamically consistent multiscale constitutive relations for unsaturated granular materials has been developed. Within this framework, the microscopic total Helmholtz free energy has been separated between a mechanical and a hydraulic part, each of which is a function of either the elastic displacement or the capillary bridge volume and the distance between particles at the micro scale. The inter-particle dissipation of energy, assumed to be frictional in origin, is a function of the incremental plastic displacements at the micro scale. Both the microscale Helmholtz free energy and the dissipative energy have been volumetrically averaged to obtain the homogenized energy functions at the macro scale. In accordance with the suggested multiscale thermomechanical framework, a micromechanical model has been constructed to describe the behavior of partially saturated granular soils. This model has considered the deformation of soil skeleton by applying a Coulomb type criterion at the inter-particle contacts. The hydraulic potential is made to be dependent on the size of the particles and is derived through use of the expression for the water retention curve by assuming that liquid bridges are isotropically distributed within the specimen. The performance of the suggested model has been demonstrated through numerical simulations of the behavior of sand under various degrees of saturation and a wide range of mechanical loadings.

Keywords: granular material ; multiscale modeling ; unsaturated soil ; micromechanical model ; thermodynamic principles

1. Introduction

Many problems in geotechnical engineering involve the interaction between the soil skeleton and the liquid. The slope stability problem, for example, is largely caused by precipitation and infiltration, so the efforts to address this issue could benefit from a deeper understanding of the behavior of unsaturated granular soils [1–3]. Unsaturated granular soils are three-phase granular materials comprising soil particles, water, and air (or soil particles and two other fluids). Thus the macroscopic behavior of unsaturated granular soils is strongly dependent on the characteristics of these components and on their interactions. Usually the solid and liquid phases are assumed to be incompressible, whereas

*. Corresponding author ; e-mail : pierre-yves.hicher@ec-nantes.fr ; tel : +33 (0)6 85 31 24 76

the gas compressible. Three interaction pairs exist : solid and liquid, solid and gas, as well as fluid and gas. These interactions appear in the form of capillary forces exerted by the water menisci on the particles. The magnitude of the capillary forces, which relates to the degree of saturation, can cause significant changes in the volume, shear strength and hydraulic properties of granular soils [4, 5].

To simulate the behavior of unsaturated soils, phenomenological models have been developed and successfully applied to solving geotechnical problems [2, 4–10]. Earlier models tended to adopt net stress and suction as independent stress variables and to extend the available elastoplastic models for saturated soils by introducing suction-dependent compressibility and yield surface [6–8]. One result of this approach was the much-celebrated Barcelona Basic Model (BBM) proposed by Alonso *et al.* [6], in which a suction-dependent loading collapse curve was introduced based on the modified Cam-Clay model. Alternatively, many attempts have been made to define an effective stress that accounts for the deformation of the soil skeleton in unsaturated soils [11–15]. Through use of the effective stress concept, the hydraulic hysteresis phenomenon and the transitional behavior from the unsaturated to the saturated state can be successfully captured [16].

From a physical point of view, the formation of water menisci between neighboring grains produces capillary forces acting on those grains. Based on this observation, the CH micromechanical framework [17] for saturated granular soils was extended to study the hydro-mechanical behavior of unsaturated granular materials [18]. In this model, the capillary forces between inter-particle contacts, assumed to depend on the degree of saturation, were integrated with the same homogenization method as for the mechanical forces. The Love-Weber formula adopted for the soil skeleton was also used to sum up the capillary forces as a tensor type capillary stress. Moreover, the same static hypothesis based localization operator was used in the hydraulic part [18–20]. It should be noted, however, that various Discrete Element Method (DEM) studies have questioned the use of the Love-Weber formula to determine the capillary stress tensor [21–25]. Furthermore, the relation between the capillary force and the degree of saturation was formulated empirically with several *ad hoc* parameters.

The capillary stress tensor, instead of the suction, was proposed to serve as a stress-like state variable representing the effects of the water menisci [19, 22, 26–28]. Because microscale capillary forces are directional vectors that cannot be generally described by a global scalar quantity, the suction cannot fully describe a multiscale system. For example, an initially isotropic unsaturated granular soil becomes anisotropic under shearing, and thus the distribution of the capillary forces may also become anisotropic, as discussed by [23, 29–31]. However, it is currently still difficult to measure the tensor type capillary stress in laboratory tests. One of the few methods available for quantifying it is the use of DEM simulations by applying the Young-Laplace equation to describe the behavior of capillary bridges in the pendular regime [19, 21, 24, 30].

Thermomechanical theory has proven to be a coherent framework within which constitutive relations can be developed through few *ad hoc* assumptions [32]. Various studies have produced thermodynamically consistent constitutive models for unsaturated soils [33–35]. In these models, effective stresses were derived through analyzing the work input for an unsaturated representative volume element (RVE), and were conjugated to the deformation of the solid skeleton [13, 14, 33, 36, 37]. However, most thermodynamically consistent models for unsaturated granular soils are based on phenomenological hypotheses [8, 13, 33].

Given the described limitations of the current constitutive relations for unsaturated granular soils, it is the aim of this paper to construct a micromechanical model for unsaturated granular soils based on thermodynamic principles. A thermodynamic approach with internal variables has been developed

and applied to the multiscale modeling of unsaturated granular soils, assuming the only source of energy dissipation to be friction occurring at inter-particle contacts during loading. The performance of the suggested model is demonstrated through numerical simulations of the behavior of sand under various degrees of saturation and a wide range of mechanical loadings.

2. Thermodynamic formulation for multiscale modeling of unsaturated granular materials

At the continuum level, thermodynamic principles involving internal variables have been applied to construct constitutive relations for partially saturated granular soils [13, 14, 36, 38]. In this study, the following assumptions adopted in the continuum models have been used : (1) solids and water are incompressible ; (2) the RVE is subjected to small deformation ; (3) the inter-phase interactions are only governed by the capillary forces. For simplicity, this study considers only the RVE under iso-thermal boundary condition, as shown in Fig. 1.

Several derivations of work input in literature are available, each of which has the purpose of establishing the work conjugacy between effective stresses and strains [13, 14, 26, 33, 35, 36, 39, 40]. However, no experimental results available to calibrate a capillary stress tensor, these studies used the suction in the work input equations. Therefore, we will not derive an expression of work input incorporating a tensor type capillary stress due to the difficulty of calibration, but we will adopt the work input formulation suggested by Houlsby [36]. Therefore, the scalar quantity suction will be used to represent the macro behavior of an RVE for unsaturated granular soils.

For an RVE of a unsaturated granular soil, denoting its porosity as n and its degree of saturation as S_r, the volume fraction of solid, water and air can be expressed as $1-n$, nS_r and $(1-S_r)n$ respectively, as also shown in Fig. 2. According to Houlsby [36], the work input of an RVE is

$$\delta W = -\mathbf{w}_w \cdot \nabla u_w^e - \mathbf{w}_a \cdot \nabla u_a^e + n(1-S_r)u_a \frac{\dot{\rho_a}}{\rho_a} - ns\dot{S}_r + [\boldsymbol{\sigma} - u_a \boldsymbol{I} + sS_r \boldsymbol{I}] : \dot{\boldsymbol{\epsilon}} \tag{1}$$

in which $\mathbf{w}_w$ and $\mathbf{w}_a$ correspond to the seepage velocities of water and air ; $\nabla u_w^e = \nabla u_w - \rho_w \mathbf{g}$ and $\nabla u_a^e = \nabla u_a - \rho_a \mathbf{g}$ are gradients of excess pore pressures ; s is the matric suction computed by $s = u_a - u_w$; the dot notation is used for differentiation. Eq. (1) indicates that several work-conjugate pairs of external variables exist. The first two terms are the relative flow velocities and are work conjugated with the gradients of excess pore pressures. The third term demonstrates that the smeared air pressure $n(1-S_r)u_a$ is conjugated with the volumetric strain rate of air $\dot{\rho_a}/\rho_a$. The fourth term is the smeared suction ns, which is work-conjugated with the rate of the degree of saturation $\dot{S}_r$. The last one displays that the quantity which is work conjugated with the strains is a stress term $\boldsymbol{\sigma} - u_a \boldsymbol{I} + sS_r \boldsymbol{I}$. This term is an expression of the effective stress tensor

$$\boldsymbol{\sigma}' = \boldsymbol{\sigma} - u_a \boldsymbol{I} + sS_r \boldsymbol{I} = \boldsymbol{\sigma}^{net} + sS_r \boldsymbol{I} \tag{2}$$

which corresponds to Bishop's [11] expression of the effective stress with the ponderation parameter χ equal to S_r. It should be mentioned that Eq. (2) does not imply that unsaturated soils can be simply described by Bishop's effective stress tensor with $\chi = S_r$ [36].

For rate-independent problems, the seepage velocities of the water and air phases are negligible, so the first two terms of Eq. (1) become zero. During conventional experimental loadings, the air pressure is usually equal to the atmospheric pressure, so it is assumed here that the air pressure remains

constant, which implies that the third term of Eq. (1) can be neglected. With these hypotheses, Eq. (1) can be further simplified as

$$\delta W = \boldsymbol{\sigma}' : \dot{\boldsymbol{\epsilon}} - ns\dot{S}_r \tag{3}$$

in which the first term represents the mechanical work input due to the deformation of the solid phase and the second term takes into account the hydraulic work input by means of changes in the water content [36, 38].

Since the deformation of a granular material originates from the relative displacement and rearrangements at the inter-particle contacts, the energy is dissipated and stored between these contacts. Given these considerations, it seems reasonable to construct a micromechanical model which is thermodynamically consistent at both the inter-particle contacts and the representative volume levels.

2.1. Macroscopic energy conservation

According to Coussy *et al.* [33], the dissipation of energy related to the change of saturation can be considered to be negligible. In other words, the hydraulic energy appears only in the formulation of the Helmholtz free energy. Generally, the hyper-elastic expression is based on two kinematic state variables, i.e., the macro strain and the degree of saturation. Additionally, we suppose that the free energy can be decomposed into two additive parts, the first Ψ^M describing the recoverable mechanical energy at the contacts, and the second Ψ^H the hydraulic energy stored in the liquid phase

$$\Psi\left(\boldsymbol{\epsilon}^e, S_r\right) = \Psi^M\left(\boldsymbol{\epsilon}^e\right) + \Psi^H\left(S_r\right) \tag{4}$$

By comparison, the dissipation energy increment ϖ is assumed to be a homogeneous function of degree 1 in terms of the plastic strain increment $\dot{\boldsymbol{\epsilon}}^p$ [32]

$$\varpi = \varpi\left(\dot{\boldsymbol{\epsilon}}^p\right) \geq 0 \tag{5}$$

By introducing the work input Eq.(3), the Helmholtz free energy function Eq.(4) and the dissipative rate function Eq. (5) into the energy conservation $\delta W = d\Psi + \varpi$, one can obtain

$$\left(\boldsymbol{\sigma}' - \frac{\partial \Psi}{\partial \boldsymbol{\epsilon}^e}\right) : \dot{\boldsymbol{\epsilon}}^e + \left(\boldsymbol{\sigma}' - \frac{\partial \varpi}{\partial \dot{\boldsymbol{\epsilon}}^p}\right) : \dot{\boldsymbol{\epsilon}}^p - \left(ns + \frac{\partial \Psi}{\partial S_r}\right)\dot{S}_r = 0 \tag{6}$$

Since Eq. (6) is satisfying for the whole representative volume, the relationship between ns and the degree of saturation is given by

$$ns = -\frac{\partial \Psi}{\partial S_r} = -\frac{\partial \Psi^H\left(S_r\right)}{\partial S_r} \tag{7}$$

And the effective stress can be obtained by

$$\boldsymbol{\sigma}' = \frac{\partial \Psi\left(\boldsymbol{\epsilon}^e, S_r\right)}{\partial \boldsymbol{\epsilon}^e} \tag{8}$$

In Eq.(6), it should be noted that the effective stress $\boldsymbol{\sigma}'$ can also be computed by $\boldsymbol{\sigma}' = \frac{\partial \varpi}{\partial \dot{\boldsymbol{\epsilon}}^p}$. However, this relation presumes that the stored energy, which is a function of the plastic strain and part of the Helmholtz free energy, is not considered, see also [32, 41].

2.2. Micro-macro energy relations

In order to derive the inter-particle contact law from thermomechanical considerations, we have constructed the relations between the work input, the free energy and the dissipation energy at the

micro and macro scales. To this purpose, the volumetric techniques for relating energy at different scales suggested by [41–44] have been adopted. The macro energy quantities are assumed to be volumetric averages of micro energy quantities

$$\delta W = \frac{1}{V}\sum_{c=1}^{N}\delta W^c, d\Psi = \frac{1}{V}\sum_{c=1}^{N} d\Psi^c \text{ and } \varpi = \frac{1}{V}\sum_{c=1}^{N}\varpi^c \tag{9}$$

in which c is the inter-particle contact defined as contacts between particles with or without the presence of liquid bridges; N is the number of particle contacts in a volume V of RVE.

Since the strain tensor can be calculated from the displacements at the inter-particle contacts [45–47], the displacement at the microscale level should be considered as an internal variable. Its work-conjugate is then the inter-particle contact force. According to experimental studies [48, 49] and analytical theories that are consistent with the Young-Laplace equation [50–52] for capillary bridge forces between spheres of equal radii, capillary bridge forces depend on the capillary bridge volume and the distance between two particles, hence the two quantities can be used as hydraulic internal variables at the microscale. The relations of the work input, Helmholtz free energy and dissipative energy at the microscale and at the macroscale are presented in Table 1.

2.3. Microscopic energy conservation

In comparison to the macroscopic mechanical free energy that depends only on elastic strain, the microscopic mechanical elastic work input is equal to the microscopic mechanical Helmholtz free energy, expressed as

$$\delta W^{cMe} = f_i^c \dot{\delta}_i^{ce} = d\Psi^{cM} = \frac{\partial \Psi^{cM}\left(\boldsymbol{\delta}^{ce}\right)}{\partial \boldsymbol{\delta}^{ce}} d\boldsymbol{\delta}^{ce} \tag{10}$$

in which $\boldsymbol{\delta}^{ce}$ is elastic displacement at the inter-particle contacts. Also at the micro scale, the plastic work input is equated to the dissipative energy, since the free energy does not depend on plastic displacements

$$\delta W^{cMp} = f_i^c \dot{\delta}_i^{cp} = \varpi^{cM} = \frac{\partial \varpi^{cM}(\dot{\boldsymbol{\delta}}^{cp})}{\partial \dot{\boldsymbol{\delta}}^{cp}} d\boldsymbol{\delta}^{cp} \tag{11}$$

where $\boldsymbol{\delta}^{cp}$ is plastic displacement at the inter-particle contacts.

Given the capillary bridge volumes and the distances between particles, the capillary bridge forces can be calculated [48–51]. Therefore, a potential expression for the hydraulic work input can be given by

$$\delta W^{cH} = f_d^{cap}\dot{\delta}^{cap} + f_v^{cap}\dot{v}^{cap} \tag{12}$$

in which δ^{cap} is the distance between two particles; $\dot{v}^{cap} = \dot{V}^{cap}/r^2$ with V^{cap} being the capillary bridge volume and r the mean radius of particles which is a material constant; f_d^{cap} and f_v^{cap} are capillary bridge forces due to the change of the particle distance and of the capillary bridge volume. Based on the adopted hypothesis that the change of water amount will not dissipate the energy, the microscopic hydraulic work input is hence equal to the microscopic hydraulic free energy, given by

$$\delta W^{cH} = d\Psi^{cH}\left(V^{cap}, \delta^{cap}\right) = \frac{\partial \Psi^{cH}\left(V^{cap}, \delta^{cap}\right)}{\partial \delta^{cap}} d\delta^{cap} + \frac{\partial \Psi^{cH}\left(V^{cap}, \delta^{cap}\right)}{\partial V^{cap}} dV^{cap} \tag{13}$$

Substituting Eqs.(10), (11), (12) and (13) into the energy conservation $\delta W^c = d\Psi^c + \varpi^c$ at the

microscale, we obtain

$$\left(\mathbf{f}^c - \frac{\partial \Psi^{cM}}{\partial \boldsymbol{\delta}^{ce}}\right)\dot{\boldsymbol{\delta}}^{ce} + \left(\mathbf{f}^c - \frac{\partial \varpi^{cM}}{\partial \dot{\boldsymbol{\delta}}^{cp}}\right)\dot{\boldsymbol{\delta}}^{cp} + \left(f_d^{cap} - \frac{\partial \Psi^{cH}}{\partial \delta^{cap}}\right)\dot{\delta}^{cap} + \left(f_v^{cap} - r^2\frac{\partial \Psi^{cH}}{\partial V^{cap}}\right)\dot{v}^{cap} = 0 \quad (14)$$

Since Eq.(14) is satisfying for any interparticle displacement, capillary bridge volume and particle distance, it follows that

$$\mathbf{f}^c = \frac{\partial \Psi^{cM}\left(\boldsymbol{\delta}^{ce}\right)}{\partial \boldsymbol{\delta}^{ce}}, f^{cap} = f_d^{cap} + f_v^{cap} = \frac{\partial \Psi^{cH}\left(V^{cap}, \delta^{cap}\right)}{\partial \delta^{cap}} + r^2\frac{\partial \Psi^{cH}\left(V^{cap}, \delta^{cap}\right)}{\partial V^{cap}} \quad (15)$$

It should be noted that there is no available hydraulic free energy function $\Psi^{cH}(V^{cap}, \delta^{cap})$ for a liquid bridge between two spherical particles of equal size in the literature. From an experimental perspective, measuring this hydraulic energy function is particularly difficult because the hysteresis in the contact angle arises from surface roughness and heterogeneity [53, 54]. Since the geometry of a steady capillary bridge surface can be described by the Young-Laplace equation, the hydraulic free energy $\Psi^{cH}(V^{cap}, \delta^{cap})$ can be obtained by numerically solving the Young-Laplace equation with prescribed capillary bridge volume and particle distance. Because the numerical integration of the Young-Laplace equation for various capillary bridge volumes and particle distances is time-consuming, a simplified method to define the hydraulic free energy at the microscale will be used in section 3.2.

The procedure for constructing micromechanical models following the described multiscale thermomechanical framework includes : (1) defining microscopic Helmholtz free energy potentials for both the mechanical and the hydraulic parts, and the dissipative rate function for the mechanical part ; (2) deriving the elastic/plastic relations from the energy potentials (it is worth mentioning that the Ziegler's orthogonality condition [55], according to which the dissipative force is outward normal to the dissipation surface, has been adopted as a way of relating the dissipative variables to the dissipation potential, and to deduce the inter-particle yield criterion and flow rule from the microscopic dissipative rate function) ; (3) establishing the micro-macro relation of strain in terms of the inter-particle displacements ; (4) deriving the effective stress tensor which is the work conjugate to the total strain tensor. In the following subsections, a micromechanical model will be constructed (as an example) to demonstrate the usefulness of this multiscale thermomechanical framework.

3. A thermodynamic micromechanical model for unsaturated granular materials

In this section, a thermodynamically consistent micromechanical model has been developed for unsaturated granular materials under the thermomechanical framework. Therefore, the CH micromechanical model has been slightly modified to describe the mechanical behavior and a hydraulic free energy potential has been suggested to account for capillary cohesion.

3.1. Mechanical potentials at the micro scale

Since the macro elastic and plastic behaviors originate from relative displacements of contacting particles, the inter-particle displacement can be divided into two parts : elastic (recoverable) and plastic (irrecoverable). In order to facilitate the micro to macro transition, a local coordinate system (n, s, t) has been defined, as shown in Fig. 3, in which n is the normal to the contact plane, whereas s and t are orientations within the contact plane. The relationship between local and global coordinates

can be defined by the angles β and γ, which can be expressed as [56]

$$P = \begin{bmatrix} \cos\gamma & \sin\gamma\cos\beta & \sin\gamma\sin\beta \\ -\sin\gamma & \cos\gamma\cos\beta & \cos\gamma\sin\beta \\ 0 & -\sin\beta & \cos\beta \end{bmatrix} = \begin{bmatrix} n_1 & n_2 & n_3 \\ s_1 & s_2 & s_3 \\ t_1 & t_2 & t_3 \end{bmatrix} \tag{16}$$

Therefore, the quantities defined at inter-particle contacts can be expressed globally by Eq.(16).

3.1.1. Inter-particle hyperelasticity

Hyperelasticity guarantees that the granular material obeys the first law of thermodynamics. The behavior of the hyperelastic granular material can be defined by the Helmholtz free energy function [32]. The Helmholtz free energy potential at the micro scale can be defined as

$$\Psi^{cM}\left(\boldsymbol{\delta}^{ce}\right) = \frac{1}{2}k_n^c\left(\delta_n^{ce}\right)^2 + \frac{1}{2}k_r^c\left(\delta_r^{ce}\right)^2 \tag{17}$$

where k_n^c and k_r^c are stiffness parameters in normal and tangential directions, which are related through

$$k_r^c = k_{rR}k_n^c \tag{18}$$

where k_{rR} is a material parameter. By differentiating Eq.(17) with respect to the displacements, the elastic inter-particle contact force-displacement relation can be obtained

$$\dot{f}_i^c = k_{ij}^c\dot{\delta}_j^{ce} \tag{19}$$

where k_{ij}^c is the elastic stiffness with $k_{nn}^c = k_n^c$, $k_{ss}^c = k_{tt}^c = k_r^c$ and $k_{ij}^c = 0$ for $i \neq j$.

3.1.2. Inter-particle hyperplasticity

Irrecoverable displacement between grains in contact during loading requires the mechanism of plasticity to be introduced at the local level. To define the hyper-plastic part of the local law, a dissipative energy potential at the micro scale should be introduced. However, it is impossible to define this local law based on experimental observations, since the energy dissipation cannot be evaluated at this scale. Considering that the model proposed by [17] is capable of simulating with acceptable accuracy the soil response to various mechanical loadings while using only a few parameters that are easily calibrated by elementary tests, the inter-particle plastic equations of the model will be retained and its energy dissipation will be evaluated by the inverse procedure presented in section 2.3.

The Coulomb type yield criterion suggested by the CH model, which describes a frictional type energy dissipation, can be rewritten as

$$F(f_i^c, \kappa) = \sqrt{(f_s^c)^2 + (f_t^c)^2} - f_n^c\kappa(\delta_r^{cp}) \tag{20}$$

where the hardening parameter $\kappa(\delta_r^{cp})$ is dependent on the tangential plastic displacement, written as

$$\kappa(\delta_r^{cp}) = \frac{k_p^c\tan\phi_p^c\delta_r^{cp}}{f_n^c\tan\phi_p^c + k_p^c\delta_r^{cp}} \text{ with } \dot{\delta}_r^{cp} = \sqrt{(\dot{\delta}_s^{cp})^2 + (\dot{\delta}_t^{cp})^2} \tag{21}$$

where k_p^c is a function of the normal contact stiffness k_n^c with the ratio k_{pR} as a material constant

$$k_p^c = k_{pR}k_n^c \tag{22}$$

ϕ_p^c is the mobilized peak friction angle between particles in contact, and is a function of the inter-particle friction angle ϕ_μ^c and of the state variable e_c/e, concordantly with the macro scale relation proposed by [57]

$$\tan\phi_p^c = \left(\frac{e_c}{e}\right)\tan\phi_\mu^c \tag{23}$$

where e is the void ratio of the granular assembly and e_c is the void ratio at the critical state. Different from the CH model [17], an exponential critical state line that has the ability to describe the evolution of the void ratio at critical state under a wide range of confining pressure by [58] has been adopted

$$e_c = e_{ref}\cdot exp\left[-\lambda\left(p'/p_{ref}\right)^{\xi}\right] \tag{24}$$

in which e_{ref} is the void ratio and p_{ref} being an effective pressure at a reference state; λ is the compression index; ξ is a material constant; p' is the mean effective pressure.

According to [17], a local dilatancy law has been defined as the ratio between the normal plastic displacement increment and the tangential plastic displacement increment, and is a function of the dilatancy angle between particle contacts, and of the ratio between current tangential and normal forces

$$D = \frac{\dot{\delta_n^{cp}}}{\dot{\delta_r^{cp}}} = \tan\phi_d^c - \frac{\sqrt{(f_s^c)^2+(f_t^c)^2}}{f_n^c} \tag{25}$$

where the dilatancy angle ϕ_d^c is also dependent on the state variable e_c/e and the inter-particle friction angle

$$\tan\phi_d^c = \left(\frac{e}{e_c}\right)\tan\phi_\mu^c \tag{26}$$

where ϕ_μ^c is the friction angle between particles, a material constant. ϕ_p^c and ϕ_d^c control the evolution of strength and the deformation at the particle contacts, as also described by [59, 60].

In order to examine the hyper-plasticity condition, the plastic work and the dissipative energy should be calculated. According to the definition in Eq. (21), the micro-scale plastic work can be expressed as

$$\delta W^{cMp} = f_n^c d\delta_n^{cp} + f_r^c d\delta_r^{cp} \tag{27}$$

From the expression of the yield criterion in Eq.(20), its partial derivatives can be written as

$$\frac{\partial F}{\partial f_n^c} = -\frac{\kappa^2(\delta_r^{cp})}{\tan\phi_p^c}, \frac{\partial F}{\partial f_s^c} = \frac{f_s^c}{\sqrt{(f_s^c)^2+(f_t^c)^2}}, \frac{\partial F}{\partial f_t^c} = \frac{f_t^c}{\sqrt{(f_s^c)^2+(f_t^c)^2}} \tag{28}$$

Since a non-associated flow rule expressed by Eq.(25) has been adopted, the partial derivatives of the potential function can be expressed as

$$\frac{\partial G}{\partial f_s^c} = \frac{\partial F}{\partial f_s^c}, \frac{\partial G}{\partial f_t^c} = \frac{\partial F}{\partial f_t^c}, \frac{\partial G}{\partial f_n^c} = D\frac{\partial G}{\partial f_r^c} = D\sqrt{\left(\frac{\partial G}{\partial f_s^c}\right)^2+\left(\frac{\partial G}{\partial f_t^c}\right)^2} = D \tag{29}$$

where G is the potential function defined at the inter-particle contacts. The plastic displacement increment can be deduced

$$d\delta_i^{cp} = \lambda^c\frac{\partial G}{\partial f_i^c} \tag{30}$$

in which λ^c is a loading index. Combining Eqs.(28) and (29), we obtain

$$\frac{\partial G}{\partial f_r^c} = \sqrt{\left(\frac{\partial G}{\partial f_s^c}\right)^2 + \left(\frac{\partial G}{\partial f_t^c}\right)^2} = 1 \tag{31}$$

Substituting Eq.(31) into Eq.(30), the relation between the loading index λ^c and the plastic displacement increment can be given as

$$\lambda^c = d\delta_r^{cp} \tag{32}$$

By including the dilatancy relationship of Eq.(25) and Eq.(32) into Eq.(27), we obtain

$$\delta W^{cMp} = f_n^c d\delta_n^{cp} + f_r^c d\delta_r^{cp} = f_n^c d\delta_r^{cp}\left(\tan\phi_d^c - \frac{f_r^c}{f_n^c}\right) + f_r^c d\delta_r^{cp} = f_n^c \tan\phi_d^c d\delta_r^{cp} \tag{33}$$

The normal force f_n^c at particle contact is always compressive and, therefore, positive; $\tan\phi_d^c$ can be proven to be positive from Eq.(26), and finally, $d\delta_r^{cp}$, as the tangential plastic increment, is also positive, as shown in Eq.(21). Therefore, the plastic work increment calculated from Eq.(27) is non-negative. Thus, the dissipation energy increment is non-negative at both micro and macro scales

$$\varpi^c = \delta W^{cMp} = f_n^c \tan\phi_d^c d\delta_r^{cp} \geq 0 \text{ and } \varpi = \frac{1}{V}\sum_{c=1}^{N} \varpi^c(\dot{\boldsymbol{\delta}}^{cp}) \geq 0 \tag{34}$$

The second law of thermodynamics is satisfied at the macro and micro scales. Hence, we can say that the mechanical part of the micromechanical model is thermodynamically consistent.

3.2. Hydraulic potential at the micro scale

Assuming that the water bridges are isotropically distributed within the material, we can use the degree of saturation as a scalar quantity to describe the change of the capillary bridge volume. In addition, considering that the interparticle normal displacements and the capillary bridge separations are both distances between particles, the separations between particles can be approximated by the inter-particle normal displacements. Therefore, the hydraulic free energy at the microscale $\Psi^{cH}(V^{cap}, \delta^{cap})$ can be equivalently represented by $\Psi^{cH}(S_r, \delta_n^c)$. As a result, the globally isotropic hydraulic behavior of unsaturated granular soils can be captured by the change of the degree of saturation S_r, while the local anisotropic hydraulic property can be described by the distribution and evolution of the interparticle normal displacements.

Several attempts have been made to define the hydraulic energy potential for unsaturated soils at the macro scale using the soil water retention curve (SWRC) [12, 33, 61]. Considering that the capillary force between two grains is a decreasing function of the distance between the grains [18, 50], the following function has been suggested for the hydraulic free energy at the inter-particle scale

$$\Psi^{cH}(S_r, \delta_n^c) = \Psi_{ref}^{cH}(S_r)\, exp\left(\frac{L-2r}{r}\right) \tag{35}$$

where L is the distance between the centers of two neighboring particles, r is a representative radius of the particles, taken as $r = d_{50}/2$, d_{50} being the grain size associated to a 50% passing in a cumulative grain size distribution (Fig.4). The value of $L-2r$ (also equal to δ^{cap}) is represented by inter-particle displacements in normal direction δ_n^c with an initial value of $0.1r$, as suggested by [18]. The subscript *ref* refers to a reference state. The reference hydraulic potential Ψ_{ref}^{cH} at the microscale can be considered to be equal to a reference hydraulic potential at the macroscale, since it has been assumed that

the water bridges are isotropically distributed within the material. The reference hydraulic potential corresponds to the SWRC, which is usually expressed empirically [62–64]. In this study, the simple logarithmic form has been adopted, since it is a continuous and integrable function [61]

$$\Psi_{ref}^{cH}\left(S_r\right)=\frac{1}{2}K_w^c\left(S_r\ln S_r+\left(2-S_r\right)\ln\left(2-S_r\right)\right) \tag{36}$$

in which K_w^c is a retention curve parameter associated with the value of the air entry suction. Based on Eq.(36), the reference free energy with respect to the degree of saturation is comparable to the water retention curve, as shown in Fig.5(a). By inserting Eq.(36) into Eq.(7), we can obtain the relation between the smeared suction ns and the degree of saturation, as shown in Fig.5(b).

With the use of the principle of energy conservation, the behavior of unsaturated granular materials can be obtained from two energy potentials, i.e. the mechanical part and the hydraulic part at inter-particle contacts. This approach guarantees that the constructed micromechanical model obeys the principles of thermodynamics.

3.3. Stress and strain tensors

To relate the internal variable at macro scale (strain) to at the micro scale (displacement), the strain tensor needs to be defined. Many definitions of strain tensors have been defined based on an equivalent continuum and a best-fit method [45–47, 65, 66]. Among them, the strain tensor suggested by Liao *et al.* [47] is the one applicable for both two-dimensional and three-dimensional conditions, and has been adopted in this study to represent the relation between microscopic displacements and macroscopic strain, which is rewritten as

$$\dot{\epsilon}_{ij}=\left(\frac{1}{V}\sum_{c=1}^{N}\dot{\delta}_i^c l_n^c\right)A_{jn};A_{jn}=\left(\frac{1}{V}\sum_{c=1}^{N}l_j^c l_n^c\right)^{-1} \tag{37}$$

in which l^c is the branch length of two connecting particles; A_{jn} is a second-order fabric tensor. In their thermodynamic analysis, Li and Dafalias [67] suggested that a fabric tensor introduced from granular micromechanics to continuum theories should be scaled by the specimen volume. It can be noted that A_{jn} satisfies such unit volume requirement.

Eq.(37) represents the deformations of granular assemblies related to the displacements at inter-particle contacts and the micro-topologies of particle clusters. Differentiating the elastic strains with respect to the elastic displacements, one can obtain

$$\frac{\partial\boldsymbol{\epsilon}^e}{\partial\boldsymbol{\delta}^{ce}}=\frac{\partial\left[\left(\frac{1}{V}\sum\limits_{c=1}^{N}\delta_i^{ce}l_n^c\right)A_{jn}\right]}{\partial\delta_i^{ce}}=\frac{1}{V}l_n^c A_{jn} \tag{38}$$

Introducing Eq.(38) into the definition of the effective stress tensor based on the Helmholtz free energy in Eq.(8), and using the work input at the micro scale, we obtain

$$\boldsymbol{\sigma}'=\frac{\partial\Psi\left(\boldsymbol{\epsilon}^e,S_r\right)}{\partial\boldsymbol{\epsilon}^e}=\frac{\partial\Psi^M\left(\boldsymbol{\epsilon}^e\right)}{\partial\boldsymbol{\epsilon}^e}=\frac{1}{V}\sum_{c=1}^{N}\frac{\partial\Psi^{cM}\left(\boldsymbol{\delta}^{ce}\right)}{\partial\boldsymbol{\delta}^{ce}}\frac{\partial\boldsymbol{\delta}^{ce}}{\partial\boldsymbol{\epsilon}^e}=\frac{1}{V}\sum_{c=1}^{N}f_i^c\cdot\frac{\partial\boldsymbol{\delta}^{ce}}{\partial\boldsymbol{\epsilon}^e}=\frac{1}{V}\sum_{c=1}^{N}f_i^c l_j^c \tag{39}$$

Eq.(39) indicates that the effective stress in unsaturated granular soils can be computed through the contact stress tensor, i.e. the Love-Weber formula. It should be mentioned that Eq.(39) is obtained from the kinematic assumption of Eq.(37), as well as the developed multiscale thermomechanical framework

given by the work input in Eq.(3). The generalization of Eq. (39) to be an effective stress tensor for partially saturated materials is a topic of current interest, which has recently been investigated through DEM simulations [21, 22, 24].

3.4. Homogenization method

The practical application of this model requires numerous summations over all the contacts $\sum_{c=1}^{N} F^c$, for any given function or variable F^c defined at inter-particle level. However, the large number of particle contacts in an RVE increases the difficulty of this summation. In this study, a spherical harmonic expansion distribution density function $\xi(\gamma,\beta)$ has been adopted to represent a discrete random granular packing, as suggested by [17]. Thus, the discrete properties can be written in a continuous way

$$\frac{1}{N}\sum_{c=1}^{N} F^c = \frac{1}{4\pi}\int_0^{2\pi}\int_0^{\pi} F(\gamma,\beta)\xi(\gamma,\beta)\sin\gamma d\gamma d\beta \tag{40}$$

where γ and β are the coordinates angles defined in Fig.3. The directional distribution density function $\xi(\gamma,\beta)$ satisfies $\oint_\Omega \xi(\gamma,\beta)\, d\Omega = 1$ in which $d\Omega = \sin\gamma d\gamma d\beta$. For an isotropic packing, the density function is equal to $1/4\pi$ [17].

In order to integrate the right-hand side of Eq.(40), the Gauss integration method has been adopted. The integral of the function $u(x,y,z)$ over a unit sphere is

$$\frac{1}{4\pi}\oint_{S^2} u(x,y,z)ds = \frac{1}{4\pi}\int_0^{2\pi}\int_0^{\pi} u(x,y,z)\sin\gamma d\gamma d\beta = \sum_{\alpha=1}^{NP} u(x,y,z)w(\alpha) \tag{41}$$

where NP is the number of integration points. The influence of NP on the accuracy of the integration has been investigated and it was found that 400 integration points over a unit sphere was enough to obtain accurate results, as discussed by [56, 68]. Through combining Eqs.(40) and (41), and by considering an isotropic fabric condition, the volumetric average of the micro variables can be calculated as

$$\frac{1}{V}\sum_{c=1}^{N} F^c = \frac{N}{4\pi V}\int_0^{2\pi}\int_0^{\pi} F(\gamma,\beta)\sin\gamma d\gamma d\beta = \frac{N}{V}\sum_{\alpha=1}^{NP} F(\alpha)w(\alpha) \tag{42}$$

where the number of contacts per unit volume N/V for a packing of spheres can be obtained from the void ratio, the average coordination number C_n and the particle size [68–70]

$$\frac{N}{V} = \frac{3C_n}{4\pi r^3(1+e)} \text{ with } C_n = 13.28 - 8e \tag{43}$$

It should be noted that both the current model and the model in [18] have adopted the strain tensor of [47] and the same Coulomb type yield criterion at the inter-particle scale. The main differences between these two models are : (1) the inter-particle elastic relation ; (2) the critical state line for the solid phase ; (3) the scalar suction s with the current model instead of the capillary stress tensor $\boldsymbol{\sigma}^{cap}$ in [18] ; (4) a free energy function for the hydraulic behavior instead of an empirical function of the degree of saturation S_r in [18]. Consequently, thermodynamic principles are satisfied by the current model.

3.5. Implementation scheme

One of the difficulties in integrating the constitutive models for unsaturated granular materials expressed by the effective stress tensor is that the experiments usually consider other forms of stress

variables such as the net stress tensors ; therefore, the constraints imposed on laboratory specimens cannot be directly specified numerically. In addition, experiments with different combinations of net stress tensors and hydraulic controls, such as suction control, drying and wetting paths and constant water content require algebraic efforts in numerical simulations. A general approach to circumvent these difficulties is to express these constraints using the linearized integration method suggested by Bardet and Choucair [71]. This method has been successfully applied to integrate an effective tensor-based model for partially saturated soils that is capable of imposing various loading programs [61], and which has thus been adopted in this study to integrate the constructed micromechanical model.

4. Performance of the model for granular soils with various degrees of saturation

In this section, the capability of the developed model to simulate the behavior of granular soils under various degrees of saturation has been evaluated. Since a critical state line applicable to crushable granular materials has been introduced, it was decided at first to calibrate the model for the crushable Dog's bay sand. Thereafter, the experimental behavior of unsaturated Chiba sand under constant water content loading was simulated by the developed model.

4.1. Dog's bay sand

In order to test the capability of the constructed micromechanical model to capture the behavior of crushable granular soils, we conducted a numerical simulation of laboratory tests on Dog's bay sand [72, 73]. According to Kuwajima *et al.* [73], Dog's bay sand is a carbonate sand from the west coast of Eire. Its specific gravity is 2.72, and its maximum and minimum void ratios are 2.451 and 1.621 respectively. A value of d_{50} of 0.22 mm is deduced from the particle size distribution shown in Fig. 6.

The critical state lines were obtained by Coop [74] through constant mean effective stress tests, as shown in Fig.7. The critical state curve in the e-$\log p'$ plane is calibrated by Eq.(24) with the parameters : $e_{ref} = 3.35$, $\lambda = 0.31$, $\xi = 0.29$ with $p_{ref} = 10$ kPa. Through Eq.(24), grain breakage can be considered implicitly by a curvilinear critical state line for the higher pressures [57]. The critical state line in the p'-q plane has a slope of $M = 1.60$, which corresponds to a friction angle of 39° (Fig. 7(b)).

The radius of the particles r is considered to be half of the diameter $d_{50} = 0.22$ mm. The parameters at the inter-particle contacts k_n^c, k_{rR} and k_{pR} were calibrated from drained triaxial compression tests performed by Kuwajima *et al.* [73] on dense Dog's bay sand with a relative density of 90%. A total of 8 parameters was required for Dog's bay sand, as summarized in Table 2. The model performed well in simulating the behavior of Dog's bay sand at various confining pressures, as shown in Fig. 8.

4.2. Chiba sand

According to Fern *et al.* [75], Chiba sand is a poorly graded silica sand with a particle size ranging from 0.01 to 1.00 mm. It has a coefficient of uniformity of 2.1 and a coefficient of curvature of 1.1. The grain size distribution was obtained by sieving and sedimentation, as shown in Fig. 9(a). The minimum and maximum void ratios are 0.500 and 0.946, respectively, and its specific gravity is 2.72. Its critical state friction angle was found to be 30°, which is a typical value for silica sand.

The water retention curve was obtained for the drying path with three different densities using the axis translation technique [75]. The specimens were subjected to matric suctions of 2 to 60 kPa. Pressures ranging from 2 to 10 kPa were applied by means of a negative water head and 60 kPa with a pressure plate. Additional investigations were carried out on a loose specimen. The air entry value

K_w^c was found to be 0.5 kPa, and the residual degree of saturation is around 20%. A small hysteresis has been observed, as shown in Fig. 9(b).

A series of triaxial tests at constant water contents were conducted on Chiba sand under vertical strain rates of 0.1%/min and 5.0%/min [75]. In this study, the long duration tests, which can be viewed as quasi-static loading tests, were adopted to calibrate the micromechanical model. The specimens with various densities, and gravimetric water contents of 10% and 17%, were sheared until an axial strain of 20% was reached. For a value of water content, three tests were carried out with an initial net mean pressure of 20 kPa, 40 kPa and 80 kPa, respectively. The detailed loading program is shown in Table 3.

The maximum effective stress ratio q/p' was found to be 1.455 (Fig.10(a)), which corresponds to a critical state friction angle of 33°. Accordingly, the friction angle at inter-particle contacts is assumed to be 33°. The critical state line was calibrated from the e-$\log p'$ plot (Fig. 10 (b)), which yielded : $e_{ref} = 1.23$, $\lambda = 0.25$ and $\xi = 0.2$, with a reference pressure of $p_{ref} = 10$ kPa. The radius of the particles r is half of the diameter $d_{50} = 0.16$ mm. The air entry value for the hydraulic free energy K_w^c is 0.5 kPa. The parameters at the inter-particle contacts k_n^c, k_{rR} and k_{pR} were calibrated from the constant water content triaxial compression tests. A total of 8 parameters were required by the micromechanical model for Chiba sand as summarized in Table 4.

The constraints used to simulate the constant water content triaxial compression tests are : $\Delta\sigma_2^{net} = \Delta\sigma_3^{net} = 0$, $\Delta\epsilon_1 = 20\%$, and $\Delta e_w = 0$ with e_w being the void ratio of water which is given by $e_w = eS_r$. Using this relation, the constant water content $\Delta w = 0$ was conducted by the condition of $\Delta e_w = 0$. The net stress term $\Delta\sigma_2^{net} = \Delta\sigma_3^{net} = 0$ was rewritten as $\Delta\sigma_2' - sS_r = \Delta\sigma_3' - sS_r = 0$, thus, the effective stress can be obtained. With these boundary conditions, the model was integrated through the linearized integration method suggested by Bardet and Choucair [71].

The simulation results are presented with experimental data in Figs. 11 and 12. The strain hardening and dilative behavior, the peak strength and the softening behavior are well captured by the micromechanical model. In terms of the plots of the shearing stress with respect to the axial loading, the model demonstrates a very good predictive capability over wide ranges of densities, confining pressures and water contents (Figs. 11(a, c, e) and 12(a, c, e)). By contrast, the model reproduces the volumetric deformation with acceptable differences between the simulation results and the experimental data. As explained by Fern *et al.* [75], the differences obtained for the dense sample are largely due to the occurrence of strain localization. Moreover, one can see that the increase of water content from 10% to 17% does not greatly influence the stress-strain behavior of Chiba sand. A possible reason is that the initial net mean pressures P_0^{net} are limitied to 20, 40 and 80 kPa. In comparison with the elasto-plastic models based upon classical continuum mechanics [8, 10, 75], not so many parameters are required for this model, and all of them have physical origins.

5. Conclusions

This paper has presented a thermodynamically consistent micromechanical model for granular materials over a wide range of saturation conditions. A thermodynamic approach with internal variables has been developed as a general framework for multiscale modeling of unsaturated granular materials. At the macro scale, the work input derived by Houlsby [36] was adopted and the Helmholtz free energy function was separated between a mechanical and a hydraulic part. The energy quantities defined at the micro and macro scales were analyzed, and the Helmholtz free energy at the microscale was also defined as the sum of a mechanical part and a hydraulic part. The free energy is dependent on the

elastic strains and on the degree of saturation at the macro scale. This translates to a dependence on elastic displacements and the capillary bridge volumes and the distances between particles at the micro scale. The dissipation energy is frictional in origin and a function of the incremental plastic displacements at the micro scale and of the incremental plastic strains at the macro scale.

A micromechanical model for unsaturated granular soils has been constructed based on the suggested multiscale thermodynamic framework. At the micro scale, a hyperelastic relation has been defined and a Coulomb type yield criterion suggested by [17] has been employed to represent the behavior of particle interactions, whereas a particle-size dependency function has been suggested to consider the water retention in the hydraulic free energy potential, allowing a simple coupling of hydro-mechanical interactions at the free energy level. At the macro scale, a critical state line, capable of describing the critical state of granular materials under a wide range of pressures, has been adopted. By using the developed thermodynamic framework, it was found that the effective stress is consistent with the Love-Weber formula. The model was tested against experimental data, demonstrating a satisfactory performance in capturing the behavior of a crushable Dog's bay sand at various confining pressures and of an unsaturated Chiba sand under triaxial compression at constant water content.

Acknowledgments

Chao-Fa Zhao acknowledges the financial support by the international scientific network GDRI GeoMech (Multi-Physics and Multi-Scale Couplings in Geo-Environmental Mechanics), and the helpful suggestions from Prof. Anil Misra (The University of Kansas) and Dr. Jian Li (Beijing Jiaotong University). Zhen-Yu Yin acknowledges the financial support by the Natural Science Foundation of China (No. 51579179).

References

[1] S. E. Cho, S. R. Lee, Instability of unsaturated soil slopes due to infiltration, Computers and Geotechnics 28 (3) (2001) 185–208.

[2] D. G. Fredlund, H. Rahardjo, M. D. Fredlund, Unsaturated soil mechanics in engineering practice, John Wiley & Sons, 2012.

[3] C. W. W. Ng, Q. Shi, A numerical investigation of the stability of unsaturated soil slopes subjected to transient seepage, Computers and Geotechnics 22 (1) (1998) 1–28.

[4] A. Gens, Soil-environment interactions in geotechnical engineering, Géotechnique 60 (1) (2010) 3.

[5] D. Sheng, Review of fundamental principles in modelling unsaturated soil behaviour, Computers and Geotechnics 38 (6) (2011) 757–776.

[6] E. E. Alonso, A. Gens, A. Josa, A constitutive model for partially saturated soils, Géotechnique 40 (3) (1990) 405–430.

[7] Y. J. Cui, P. Delage, Yeilding and plastic behaviour of an unsaturated compacted silt, Géotechnique 46 (2) (1996) 291–311.

[8] D. Sheng, S. W. Sloan, A. Gens, A constitutive model for unsaturated soils : thermomechanical and computational aspects, Computational Mechanics 33 (6) (2004) 453–465.

[9] D. Sun, D. Sheng, S. W. Sloan, Elastoplastic modelling of hydraulic and stress–strain behaviour of unsaturated soils, Mechanics of Materials 39 (3) (2007) 212–221.

[10] S. J. Wheeler, V. Sivakumar, An elasto-plastic critical state framework for unsaturated soil, Géotechnique 45 (1) (1995) 35–53.

[11] A. W. Bishop, G. Blight, Some aspects of effective stress in saturated and partly saturated soils, Géotechnique 13 (3) (1963) 177–197.

[12] G. Buscarnera, I. Einav, The yielding of brittle unsaturated granular soils, Géotechnique 62 (2) (2012) 147.

[13] J. Li, Z.-Y. Yin, Y. Cui, P.-Y. Hicher, Work input analysis for soils with double porosity and application to the hydromechanical modeling of unsaturated expansive clays, Canadian Geotechnical Journal 54 (2) (2016) 173–187.

[14] C. G. Zhao, Y. Liu, F. P. Gao, Work and energy equations and the principle of generalized effective stress for unsaturated soils, International Journal for Numerical and Analytical Methods in Geomechanics 34 (9) (2010) 920–936.

[15] E. E. Alonso, J.-M. Pereira, J. Vaunat, S. Olivella, A microstructurally based effective stress for unsaturated soils, Géotechnique 60 (12) (2010) 913–925.

[16] M. Nuth, L. Laloui, Effective stress concept in unsaturated soils : clarification and validation of a unified framework, International Journal for Numerical and Analytical Methods in Geomechanics 32 (7) (2008) 771–801.

[17] C. S. Chang, P. Y. Hicher, An elasto-plastic model for granular materials with microstructural consideration, International Journal of Solids and Structures 42 (14) (2005) 4258–4277.

[18] P.-Y. Hicher, C. S. Chang, A microstructural elastoplastic model for unsaturated granular materials, International Journal of Solids and Structures 44 (7-8) (2007) 2304–2323.

[19] L. Scholtès, P.-Y. Hicher, F. Nicot, B. Chareyre, F. Darve, On the capillary stress tensor in wet granular materials, International Journal for Numerical and Analytical Methods in Geomechanics 33 (10) (2009) 1289–1313.

[20] C.-F. Zhao, Y. Salami, Z.-Y. Yin, P.-Y. Hicher, A micromechanical model for unsaturated soils based on thermodynamics, in : Poromechanics VI, 2017, pp. 594–601.

[21] C. Chalak, B. Chareyre, E. Nikooee, F. Darve, Partially saturated media : from dem simulation to thermodynamic interpretation, European Journal of Environmental and Civil Engineering 21 (7-8) (2017) 798–820.

[22] J. Duriez, R. Wan, Stress in wet granular media with interfaces via homogenization and discrete element approaches, Journal of Engineering Mechanics 142 (12) (2016) 04016099.

[23] K. Wang, W. Sun, Anisotropy of a tensorial bishops coefficient for wetted granular materials, Journal of Engineering Mechanics 143 (3) (2015) B4015004.

[24] J.-P. Wang, X. Li, H.-S. Yu, Stress–force–fabric relationship for unsaturated granular materials in pendular states, Journal of Engineering Mechanics 143 (9) (2017) 04017068.

[25] C. Yuan, B. Chareyre, F. Darve, Deformation and stresses upon drainage of an idealized granular material, Acta Geotechnica (2017) 1–12.

[26] Y. Jiang, I. Einav, M. Liu, A thermodynamic treatment of partially saturated soils revealing the structure of effective stress, Journal of the Mechanics and Physics of Solids 100 (2017) 131–146.

[27] X. S. Li, Effective stress in unsaturated soil : a microstructural analysis, Géotechnique 53 (2) (2003) 273–277.

[28] N. Lu, Is matric suction a stress variable ?, Journal of Geotechnical and Geoenvironmental Engineering 134 (7) (2008) 899–905.

[29] J. Duriez, R. Wan, M. Pouragha, F. Darve, Revisiting the existence of an effective stress for wet granular soils with micromechanics, International Journal for Numerical and Analytical Methods in Geomechanics 42 (8) (2018) 959–978.

[30] J. Duriez, R. Wan, Subtleties in discrete-element modelling of wet granular soils, Géotechnique 67 (4) (2016) 365–370.

[31] R. Wan, S. Khosravani, M. Pouragha, Micromechanical analysis of force transport in wet granular soils, Vadose Zone Journal 13 (5).

[32] G. T. Houlsby, A. M. Puzrin, Principles of hyperplasticity : an approach to plasticity theory based on thermodynamic principles, Springer Science & Business Media, 2007.

[33] O. Coussy, J.-M. Pereira, J. Vaunat, Revisiting the thermodynamics of hardening plasticity for unsaturated soils, Computers and Geotechnics 37 (1-2) (2010) 207–215.

[34] P. Dangla, J.-M. Pereira, A thermodynamic approach to effective stresses in unsaturated soils incorporating the concept of partial pore deformations, Vadose Zone Journal 13 (5).

[35] X. S. Li, Thermodynamics-based constitutive framework for unsaturated soils. 1 : Theory, Géotechnique 57 (5) (2007) 411–422.

[36] G. Houlsby, The work input to an unsaturated granular material, Géotechnique 47 (1) (1997) 193–6.

[37] R. I. Borja, On the mechanical energy and effective stress in saturated and unsaturated porous continua, International Journal of Solids and Structures 43 (6) (2006) 1764–1786.

[38] Y. Zhang, Effect of water-particle interactions on the crushing of granular materials, Ph.D. thesis, Northwestern University (2016).

[39] M. Hassanizadeh, W. G. Gray, et al., General conservation equations for multi-phase systems : 3. constitutive theory for porous media flow, Adv. Water Resour 3 (1) (1980) 25–40.

[40] E. R. Lewis, K. Morgan, B. Schrejler, E. Hinton, P. Bettess, O. Zienkiewicz, E. C. Desai, R. Gallagher, R. Wood, J. Alex, et al., The finite element method in the deformation and consolidation of porous media.

[41] C.-F. Zhao, Z.-Y. Yin, A. Misra, P.-Y. Hicher, Thermomechanical formulation for micromechanical elasto-plasticity in granular materials, International Journal of Solids and Structures 138 (2018) 64–75.

[42] A. Misra, V. Singh, Nonlinear granular micromechanics model for multi-axial rate-dependent behavior, International Journal of Solids and Structures 51 (13) (2014) 2272–2282.

[43] A. Misra, P. Poorsolhjouy, Granular micromechanics model for damage and plasticity of cementitious materials based upon thermomechanics, Mathematics and Mechanics of Solids (2015) 1081286515576821.

[44] A. Misra, V. Singh, Thermomechanics-based nonlinear rate-dependent coupled damage-plasticity granular micromechanics model, Continuum Mechanics and Thermodynamics 27 (4-5) (2015) 787–817.

[45] K. Bagi, Analysis of microstructural strain tensors for granular assemblies, International Journal of Solids and Structures 43 (10) (2006) 3166–3184.

[46] N. P. Kruyt, L. Rothenburg, Micromechanical definition of the strain tensor for granular materials, Journal of Applied Mechanics 63 (3) (1996) 706–711.

[47] C.-L. Liao, T.-P. Chang, D.-H. Young, C. S. Chang, Stress-strain relationship for granular materials based on the hypothesis of best fit, International Journal of Solids and Structures 34 (31-32) (1997) 4087–4100.

[48] Y. I. Rabinovich, M. S. Esayanur, B. M. Moudgil, Capillary forces between two spheres with a fixed volume liquid bridge : theory and experiment, Langmuir 21 (24) (2005) 10992–10997.

[49] C. D. Willett, M. J. Adams, S. A. Johnson, J. P. Seville, Capillary bridges between two spherical bodies, Langmuir 16 (24) (2000) 9396–9405.

[50] N. P. Kruyt, O. Millet, An analytical theory for the capillary bridge force between spheres, Journal of Fluid Mechanics 812 (2017) 129–151.

[51] G. Lian, J. Seville, The capillary bridge between two spheres : New closed-form equations in a two century old problem, Advances in Colloid and Interface Science 227 (2016) 53–62.

[52] C.-F. Zhao, N. P. Kruyt, O. Millet, Capillary bridge force between non-perfectly wettable spherical particles : An analytical theory for the pendular regime, Powder Technology 339 (2018) 827–837.

[53] J. N. Israelachvili, Intermolecular and surface forces, Academic press, 2011.

[54] Y. Yuan, T. R. Lee, Contact angle and wetting properties, in : Surface science techniques, Springer, 2013, pp. 3–34.

[55] H. Ziegler, An introduction to thermomechanics, Vol. 21, Elsevier, 2012.

[56] C.-F. Zhao, Z.-Y. Yin, P.-Y. Hicher, A multiscale approach for investigating the effect of microstructural instability on global failure in granular materials, International Journal for Numerical and Analytical Methods in Geomechanics (2018) 1–30.

[57] J. Biarez, P.-Y. Hicher, Elementary mechanics of soil behaviour : saturated remoulded soils., AA Balkema, 1994.

[58] Z.-Y. Yin, Z.-X. Wu, P.-Y. Hicher, Modeling monotonic and cyclic behavior of granular materials by exponential constitutive function, Journal of Engineering Mechanics 144 (4) (2018) 04018014.

[59] Z.-Y. Yin, C. S. Chang, P.-Y. Hicher, Micromechanical modelling for effect of inherent anisotropy on cyclic behaviour of sand, International Journal of Solids and Structures 47 (14-15) (2010) 1933–1951.

[60] Z.-Y. Yin, C. S. Chang, Stress–dilatancy behavior for sand under loading and unloading conditions, International Journal for Numerical and Analytical Methods in Geomechanics 37 (8) (2013) 855–870.

[61] Y. Zhang, G. Buscarnera, Implicit integration under mixed controls of a breakage model for unsaturated crushable soils, International Journal for Numerical and Analytical Methods in Geomechanics 40 (6) (2016) 887–918.

[62] R. H. Brooks, A. T. Corey, Hydraulic properties of porous media and their relation to drainage design, Transactions of the ASAE 7 (1) (1964) 26–0028.

[63] D. G. Fredlund, A. Xing, Equations for the soil-water characteristic curve, Canadian Geotechnical Journal 31 (4) (1994) 521–532.

[64] M. T. Van Genuchten, A closed-form equation for predicting the hydraulic conductivity of unsaturated soils 1, Soil Science Society of America Journal 44 (5) (1980) 892–898.

[65] N. P. Kruyt, Statics and kinematics of discrete cosserat-type granular materials, International Journal of Solids and Structures 40 (3) (2003) 511–534.

[66] N. P. Kruyt, O. Millet, F. Nicot, Macroscopic strains in granular materials accounting for grain rotations, Granular Matter 16 (6) (2014) 933–944.

[67] X. S. Li, Y. F. Dafalias, Dissipation consistent fabric tensor definition from dem to continuum for granular media, Journal of the Mechanics and Physics of Solids 78 (2015) 141–153.

[68] C.-F. Zhao, Z.-Y. Yin, P.-Y. Hicher, Integrating a micromechanical model for multiscale analyses, International Journal for Numerical Methods in Engineering 114 (2) (2018) 105–127.

[69] C. S. Chang, A. Misra, Packing structure and mechanical properties of granulates, Journal of Engineering Mechanics 116 (5) (1990) 1077–1093.

[70] Z.-Y. Yin, J. Zhao, P.-Y. Hicher, A micromechanics-based model for sand-silt mixtures, International Journal of Solids and Structures 51 (6) (2014) 1350–1363.

[71] J. P. Bardet, W. Choucair, A linearized integration technique for incremental constitutive equations, International Journal for Numerical and Analytical Methods in Geomechanics 15 (1) (1991) 1–19.

[72] E. U. Klotz, M. R. Coop, An investigation of the effect of soil state on the capacity of driven piles in sands, Géotechnique 51 (9) (2001) 733–751.

[73] K. Kuwajima, M. Hyodo, A. F. Hyde, Pile bearing capacity factors and soil crushabiity, Journal of Geotechnical and Geoenvironmental Engineering 135 (7) (2009) 901–913.

[74] M. R. Coop, The mechanics of uncemented carbonate sands, Géotechnique 40 (4) (1990) 607–626.

[75] E. J. Fern, D. J. Robert, K. Soga, Modeling the stress-dilatancy relationship of unsaturated silica sand in triaxial compression tests, Journal of Geotechnical and Geoenvironmental Engineering 142 (11) (2016) 04016055.

Tables

Table 1: Micro-macro relations of energetic quantities

Work input	Helmholtz free energy	Dissipative energy
$\delta W = \frac{1}{V}\sum_{c=1}^{N} \delta W^c$	$d\Psi = \frac{1}{V}\sum_{c=1}^{N} d\Psi^c$	$\varpi = \frac{1}{V}\sum_{c=1}^{N} \varpi^c$
$\delta W^c = \delta W^{cM} + \delta W^{cH}$	$d\Psi^c = d\Psi^{cM} + d\Psi^{cH}$	$\varpi^c = \varpi^{cM}$
δW^{cM}	$d\Psi^{cM} = d\Psi^{ce}\left(\boldsymbol{\delta}^{ce}\right)$	$\varpi^{cM}(\dot{\boldsymbol{\delta}}^{cp}) \geq 0$
δW^{cH}	$d\Psi^{cH}\left(V^{cap}, \delta^{cap}\right)$	–

Table 2: Parameters used in the micromechanical model for Dog's bay sand

e_{ref}	λ	$k_n^c(N/mm)$	$\phi_\mu^c(^\circ)$	$d_{50}(mm)$	k_{rR}	k_{pR}
3.35	0.31	3000	39	0.22	0.6	0.4

Table 3: Initial conditions of constant water content triaxial compression tests on Chiba sand

Density	$w(\%)$	e_0	$S_r(\%)$	$p_0^{net}(kPa)$
Loose	10	0.842	32	20
	10	0.818	33	40
	10	0.808	34	80
	17	0.845	55	20
	17	0.830	56	40
	17	0.820	56	80
Medium dense	10	0.742	37	20
	10	0.738	37	40
	10	0.725	38	80
	17	0.745	62	20
	17	0.734	63	40
	17	0.719	64	80
Dense	10	0.656	41	20
	10	0.659	41	40
	10	0.653	42	80
	17	0.657	70	20
	17	0.648	71	40
	17	0.641	72	80

Table 4: Parameters used in the micromechanical model for Chiba sand

e_{ref}	λ	$k_n^c(N/mm)$	$\phi_\mu^c(^\circ)$	$d_{50}(mm)$	k_{rR}	k_{pR}	$K_w^c(kPa)$
1.23	0.25	800	33	0.16	1.0	2.0	0.5

Figures

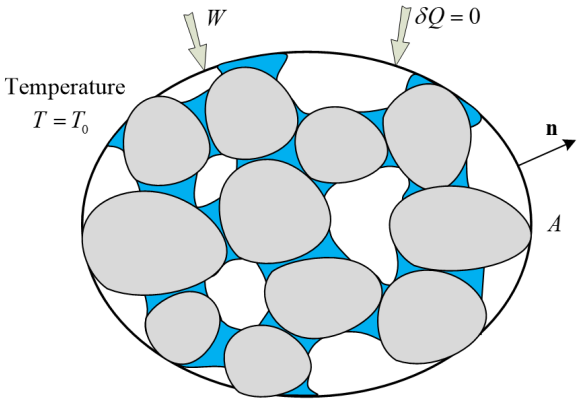

Fig. 1: RVE of unsaturated granular soils as a closed thermodynamic system.

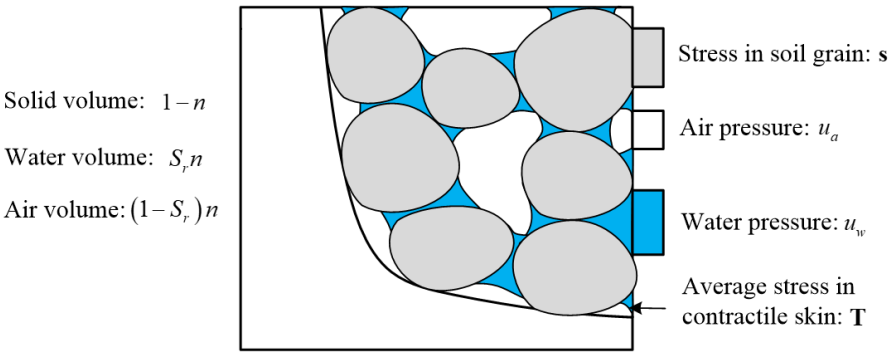

Fig. 2: Volume fractions and total stresses in an RVE of unsaturated granular soils (figure from [38]).

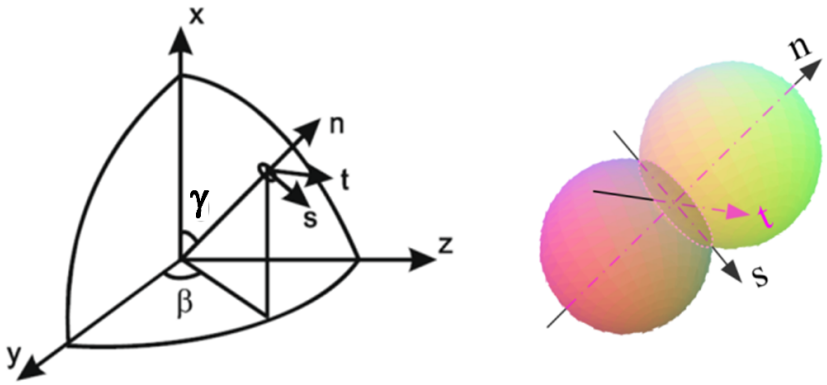

Fig. 3: Local coordinate (n, s, t) and global coordinate (x, y, z).

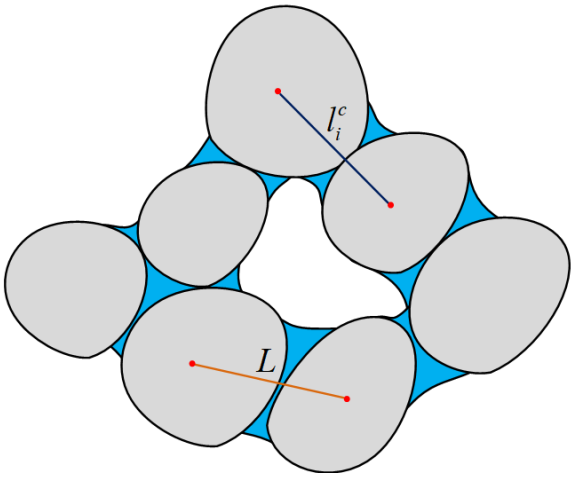

Fig. 4: Branch vector l_i^c and distance vector L.

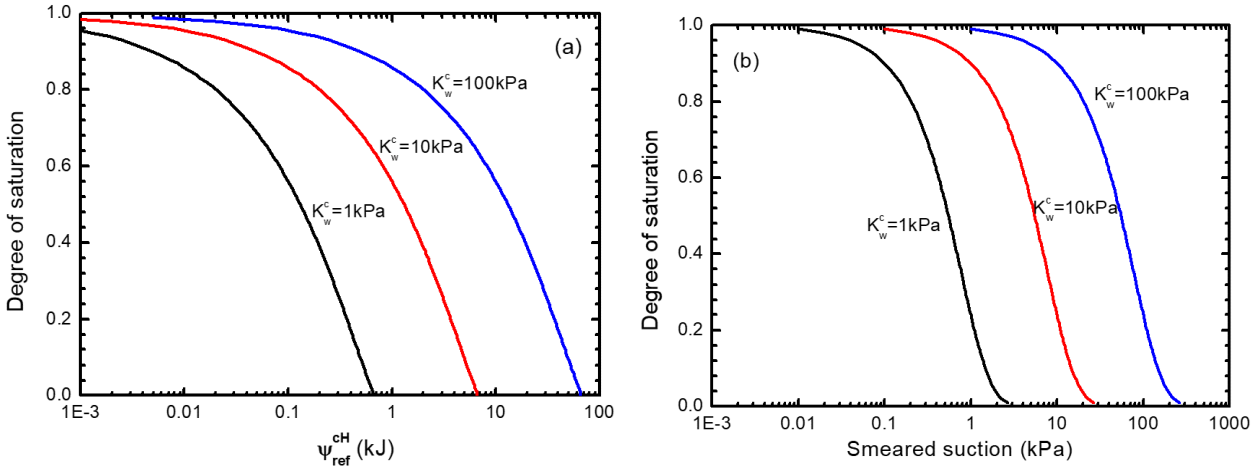

Fig. 5: Performance of the reference hydraulic potential function.

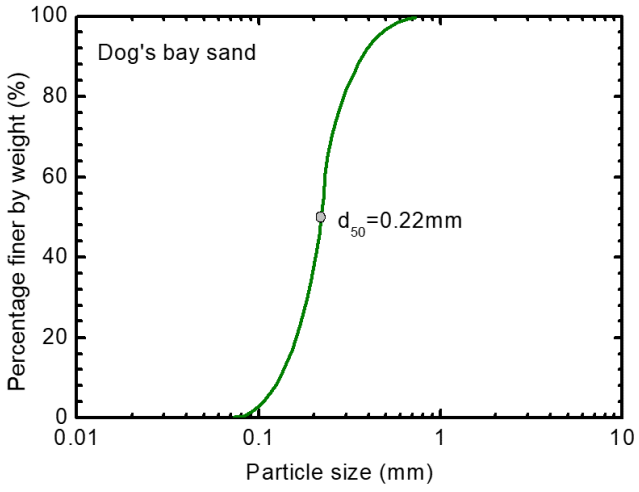

Fig. 6: Particle size distribution of Dog's bay sand (data from Kuwajima *et al.* [73]).

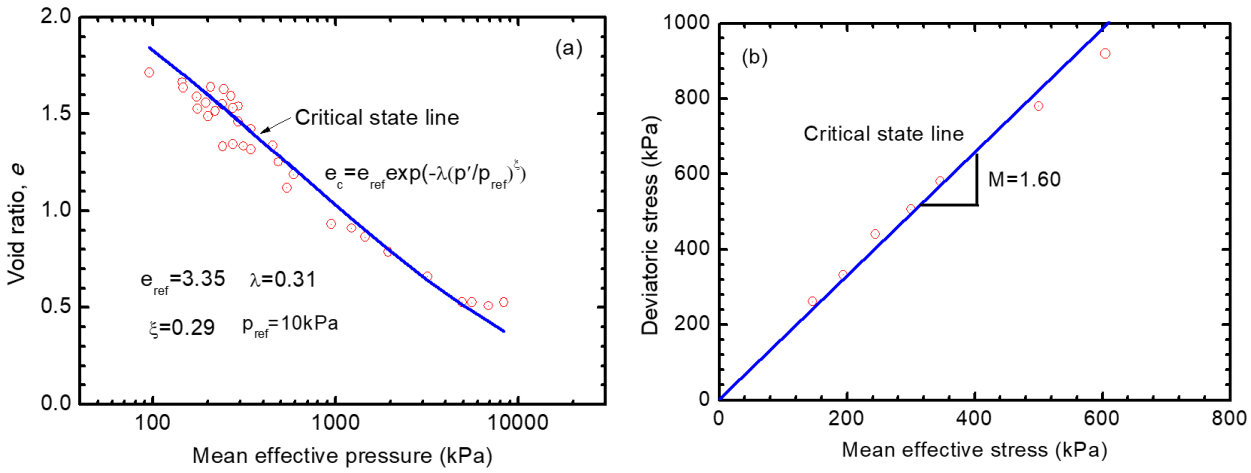

Fig. 7: Critical state lines of Dog's bay sand : (a) e-log p' plane ; (b) p'-q plane (experimental data from Coop [74]).

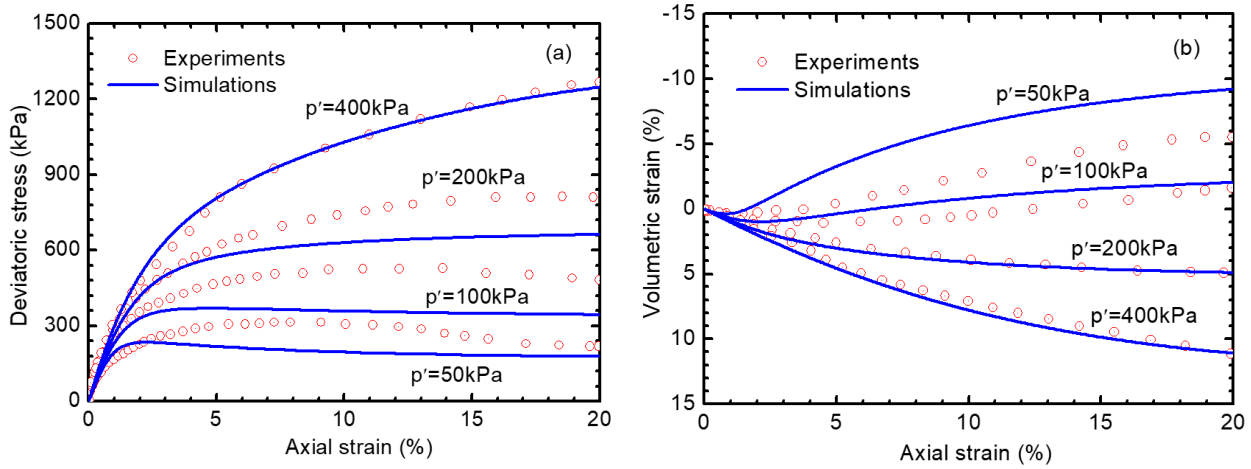

Fig. 8: Simulations of drained triaxial compression tests on Dog's bay sand : (a) deviatoric stress vs axial strain ; (b) volumetric strain vs axial strain (experimental data from Kuwajima *et al.* [73]).

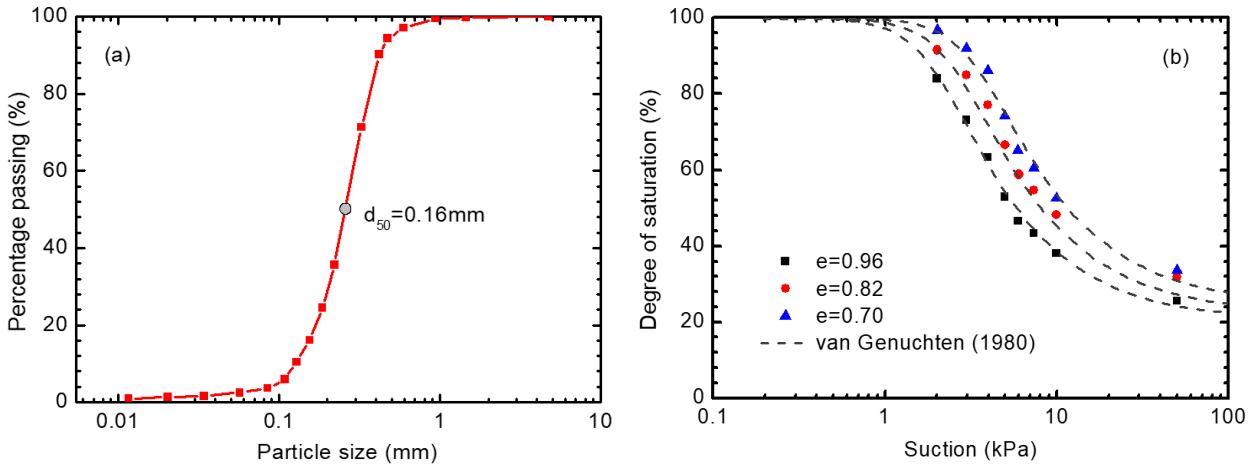

Fig. 9: Chiba sand : (a) grain size distribution ; (b) water retention curve.

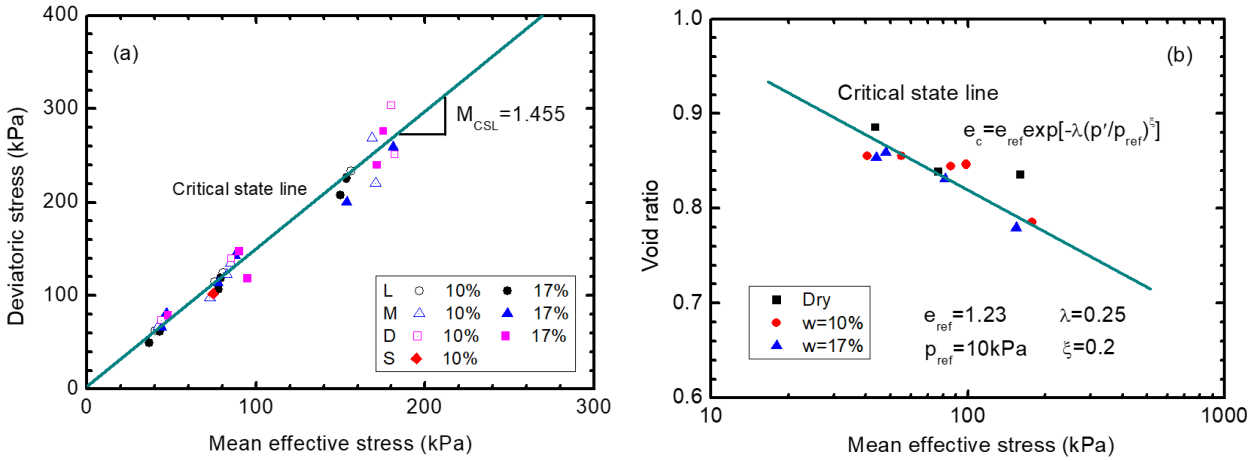

Fig. 10: Critical state lines of Chiba sand in (a) p'-q plane and (b) e-$\log p'$ plane.

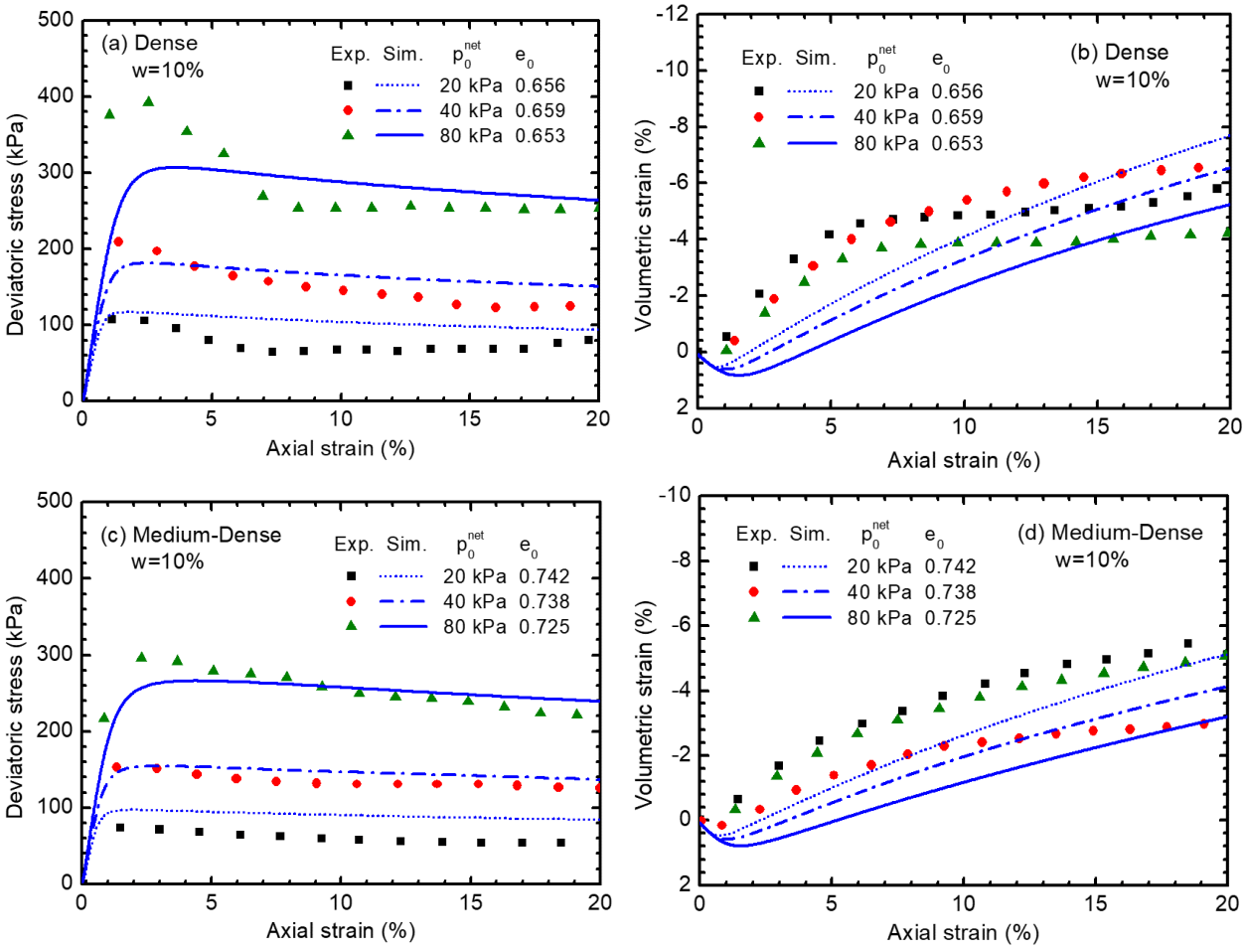

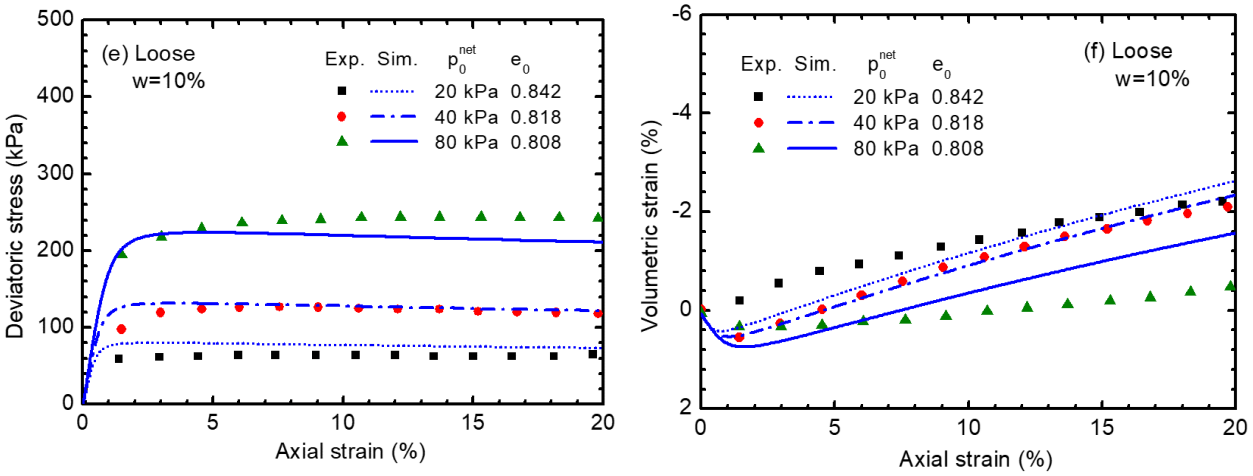

Fig. 11: Simulation of the constant water content triaxial compression tests on unsaturated Chiba sand ($w = 10\%$).

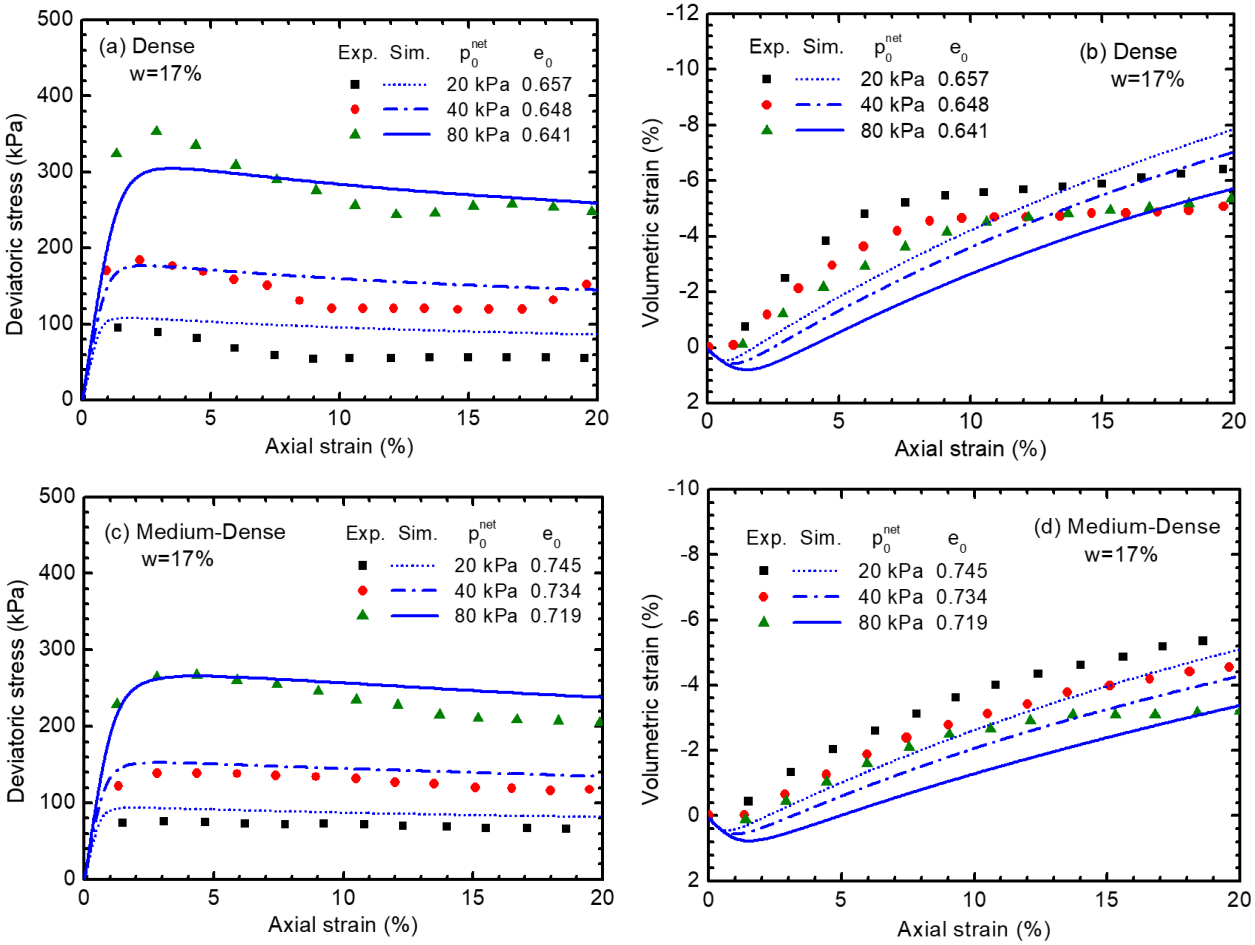

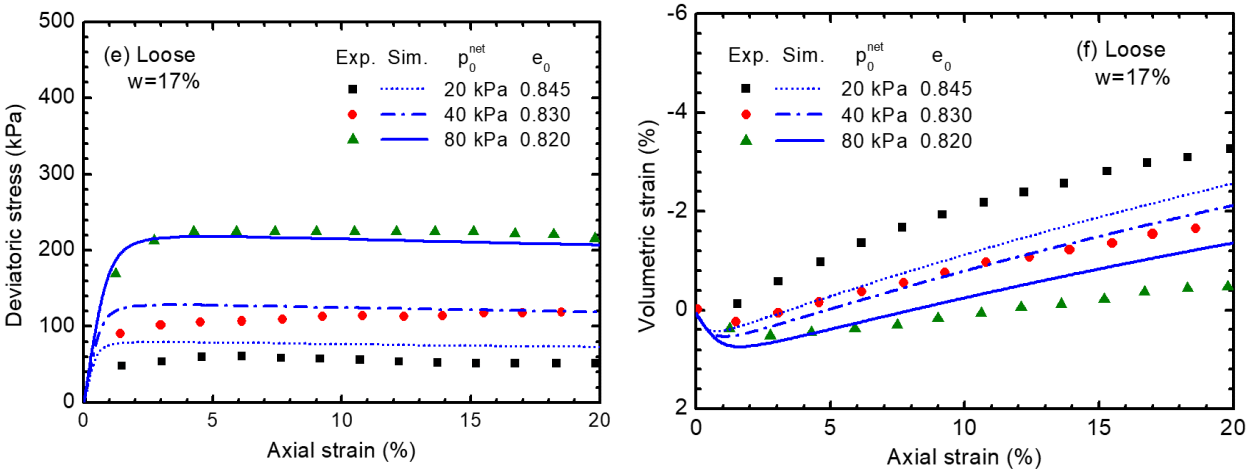

Fig. 12: Simulation of the constant water content triaxial compression tests on unsaturated Chiba sand ($w = 17\%$).